Dynamic changes in subplate and cortical plate microstructure precede the onset of cortical folding in vivo

Authors

Siân Wilson[1], Daan Christiaens[2], Hyukjin Yun[3,4], Alena Uus[1,6], Lucilio Cordero-Grande[5], Vyacheslav Karolis[1], Anthony Price[1], Maria Deprez[1,6], Jacques-Donald Tournier[1,6], Mary Rutherford[1], Ellen Grant[3,4], Joseph V. Hajnal[1,5], A David Edwards[1], Jonathan O'Muircheartaigh[1,9*], Tomoki Arichi[1,7,8], Kiho Im[3,4*]**

[1]Centre for the Developing Brain, Department of Perinatal Imaging and Health, King's College London, United Kingdom

[2]Department of Electrical Engineering, Katholieke Universiteit Leuven, Belgium

[3] Fetal Neonatal Neuroimaging and Developmental Science Center, Boston Children's Hospital, Harvard Medical School, Boston, MA 02115, USA

[4] Division of Newborn Medicine, Boston Children's Hospital, Harvard Medical School, Boston, MA 02115, USA

Boston Children's Hospital, Harvard Medical School, Boston, MA

[5]Biomedical Image Technologies, Universidad Politécnica de Madrid, Spain

[6]Department of Biomedical Engineering, School Biomedical Engineering and Imaging Sciences, King's College London, St. Thomas' Hospital, United Kingdom

[7]Department of Bioengineering, Imperial College London, United Kingdom

[8]Children's Neurosciences, Evelina London Children's Hospital, Guy's and St Thomas' NHS Foundation Trust, United Kingdom

[9]Department of Forensic and Neurodevelopmental Sciences, King's College London, United Kingdom

*co-senior authors

** corresponding author

Abstract

The structural scaffolding of the human brain is assembled during the fetal period through a series of rapid, dynamic, and intersecting processes. The third trimester of gestation is characterised by the emergence of complex patterns of cortical folding, the development of white matter connections, lamination of the cortex and formation of neural circuits. Multiple hypotheses have been proposed to explain how these processes interact to drive the formation of cortical convolutions, however there are no data-driven analyses during the fetal period to address them empirically.

To explore this gap in understanding, we quantify microstructural changes in the transient fetal compartments undergoing significant developmental change at the onset of gyrification in utero, the subplate (SP) and cortical plate (CP). Using high angular resolution multi-shell diffusion-weighted imaging (HARDI) as part of the Developing Human Connectome Project (dHCP), our analysis reveals that the anisotropic, tissue component of the diffusion signal in the SP and CP decreases immediately prior to the formation of sulcal fundi in the fetal brain. By back-projecting a map of folded brain regions onto the unfolded brain, we provide evidence for cytoarchitectural differences between gyral and sulcal areas at the end of the second trimester, suggesting that regional variation in the density and complexity of neuropil in transient fetal compartments plays a mechanistic function in the onset of folding across the brain.

Introduction

The gyrification of the human brain refers to the formation of grooves (sulci) and ridges (gyri) on the surface of the brain through the folding of the cortex. From an evolutionary perspective, it allows the expansion of cortical surface area within the confined space of the skull, optimizing the efficiency of brain circuitry by bringing interconnected cortical areas closer together, increasing the speed of information transmission (Fernandez et al., 2016). Perturbing the course of neurodevelopment can alter the folding patterns of the cerebral cortex and result in lifelong alterations in brain function, that may manifest as intellectual disability, autism, treatment-resistant epilepsy and various other cognitive or behavioural disorders (Nordahl et al., 2007, Barkovich 2012, Subramanian et al., 2020). These clinical observations motivate the need to better understand the mechanistic framework behind the early development of complex folding patterns in the cortex during the human fetal period.

At the end of the second trimester, after the bulk of neuronal migration has finished, there is a rapid increase in the rate of cortical folding across the third trimester of gestation, resulting in all major sulcal landmarks of the adult brain becoming evident by full term (Chi et al., 1977; Cachia et al., 2016; Yun et al., 2020). The deepest areas of the sulci, the sulcal pits, are the first to develop and are the most invariant across time, remaining spatially consistent even as other convolutions form (Im et al., 2010, Lohmann et al., 2008, Yun et al., 2020). It is hypothesised that the highly conserved nature of sulcal pits and primary folding patterns between individuals, compared to the secondary and tertiary sulci, would suggest that they are under closer genetic control than later developing sulci (Im & Grant 2019). By extension, the mechanisms governing the formation of cortical convolutions may differ pre- and post-natally, becoming more influenced by environmental cues at later stages of development.

Although the timeline for the prenatal development of cortical surface features has been thoroughly described, the underlying in utero biology that drives cortical folding and determines individual

variations in surface morphology is not well understood. There are many models and hypotheses about the biological mechanisms that drive cortical gyrification (Van Essen 1997, 2020, Lefèvre et al., 2010, Xu et al., 2010, Tallinen et al., 2014, 2016), which seek to explain how the fundamental processes of the second to third trimester interact dynamically to initiate the buckling of the cortex. These processes include the expansion of cortical surface area (Finlay & Darlington, 1995, Mota & Houzel, 2015), dissipation of the subplate (SP) (Rana et al., 2019), ingrowth of thalamocortical axons and white matter axonal tension (Van Essen 1997, 2020), neuronal proliferation (Kriegstein et al., 2006), regionally variant neuronal differentiation (Wang et al., 2017, Llinares Benadero & Borrell, 2019), and differential expansion of cortical layers (Richmann et al., 1975). The majority of these processes occur in the transient compartments of the fetal brain, the cortical plate (CP) and SP, which play many crucial roles in human brain development (Kostovic 2010, 2014). In this work, we examine the regional patterns of microstructural maturation in these compartments when cortical folds start to form, and test different hypotheses about their association, providing novel insight into the mechanism of cortical gyrification.

Diffusion MRI can be used to quantify structural maturation of the brain and can provide detailed information about intracellular and extracellular water diffusion over the second to third trimester. Modelling the diffusion signal allows a refined interpretation of the dynamic changes seen in image contrast in terms of the underlying cellular biology or microstructure. This has been demonstrated in rodents (Sizonenko et al., 2007, Aggarwal et al., 2015), primates (Wang et al 2017), human fetuses (Takahashi et al., 2012, 2014, Huang et al., 2014), and preterm infants (McKinstry et al., 2002, Ball et al., 2013, Batalle et al., 2019).

Using T2-weighted and high angular resolution multi-shell diffusion-weighted imaging (HARDI) data acquired as part of the open science developing Human Connectome Project (dHCP) (www.developingconnectome.org), we quantify the relationship between emerging cortical folds and the microstructural properties of the underlying tissue layers, including the CP and SP. We studied 112 imaging datasets from fetuses aged between 24 and 36 gestational weeks (GW), to quantitatively describe the relationship between sulcal formation and tissue architecture across gestational age (GA). We describe the macroscopic development of the cortex using sulcal depth, surface area and mean curvature. We then model the diffusion MR signal using a combination of the diffusion tensor imaging (DTI) and multi-shell multi-tissue constrained spherical deconvolution (MSMT-CSD), which capture different components of the diffusion signal and therefore reflect different underlying developmental processes. With the metrics derived from these models, we quantify the microstructure of the underlying SP and CP layers across the second to third trimester. Correlating these metrics at the individual subject level within developing sulci reveals a brain-wide inverse relationship between tissue fraction, the anisotropic component or ‘white-matter-like’ diffusion signal, and sulcal depth, that crucially is independent of age-related maturation. We then analyse the predictive power of microstructural change

to anticipate the emergence of cortical folds by back-projecting a map of folded brain regions onto the unfolded brain. We identified decreasing tissue fraction during the second trimester, prior to the formation of cortical folds, in regions which subsequently mature into sulcal fundi. This provides mechanistic insight into the emergence of cortical folding and the role of transient fetal compartments in this process, highlighting a critical role of neuronal and glial cellular morphological maturation in producing intracortical forces to drive the formation of primary cortical folds.

Results

General trends in surface metrics across GA

Sulcal depth, area and curvature maps demonstrated the appearance of major primary sulci over this timeframe (Figure 1a). The vertex-wise correlation between surface metrics (sulcal depth, surface area and curvature) and GA of the subject, demonstrated expected patterns of areal expansion and gyrification across the cortex (Yun et al., 2020), with high magnitude Pearson r values across the cortex (Figure 1b). Manually defined labels of 15 major primary sulci were propagated from the surface template to each subject, and the mean sulcal depth within the sulcus was charted against GA (Supplementary Figure 1). Changes in sulcal depth at each primary sulcal landmark were best fitted by sigmoidal curves over this developmental window (Supplementary Figure 1).

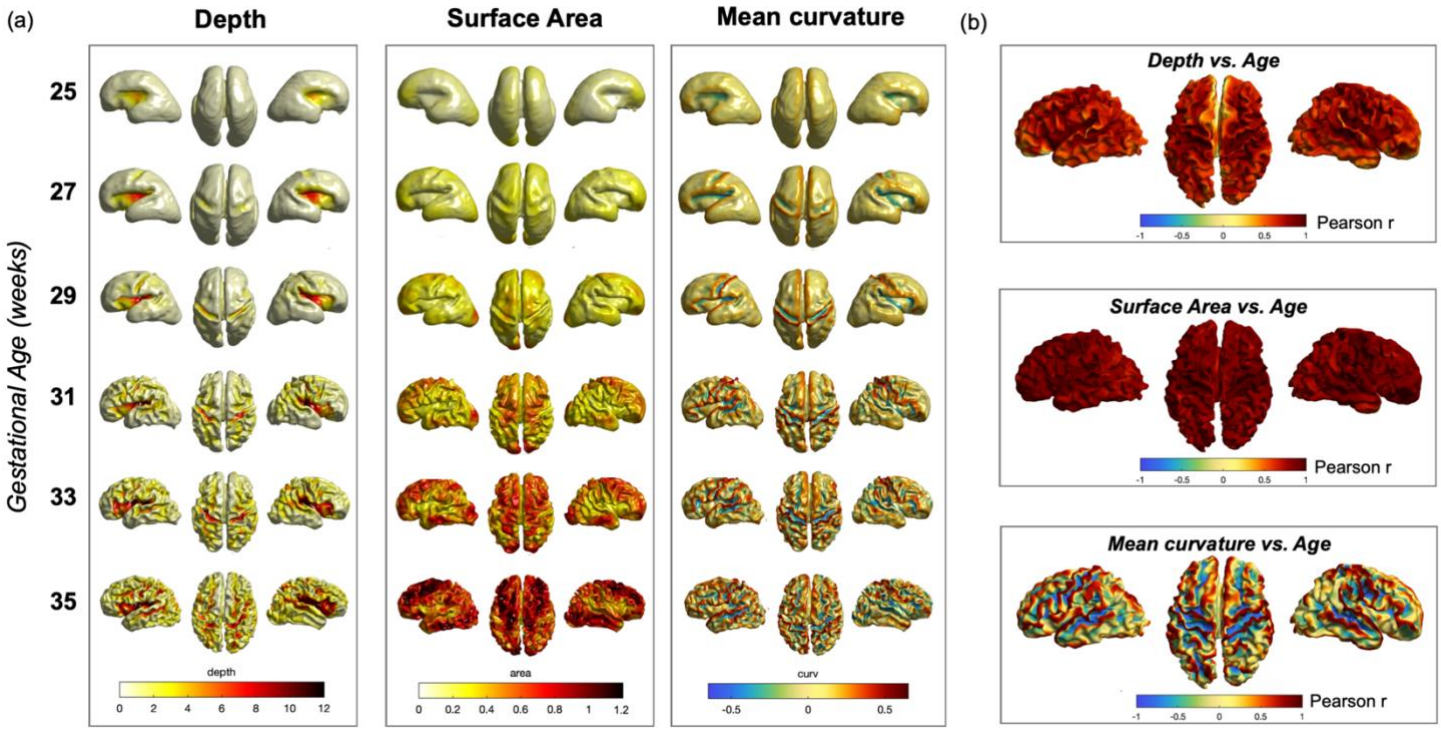

Figure 1. Age related changes in surface features (a) Mean surface metrics (depth, area, curvature) in each gestational week (b) Pearson r correlation coefficient between surface metrics and GA.

Mapping microstructural metrics to the surface and age-related trends

To quantify variations in microstructure across the cortical surface, DTI and MSMT-CSD models were both fitted to the individual subject HARDI data. Both approaches have been used to describe fetal brain maturation in previous literature (Wilson et al., 2021, Wilson et al., 2023, Jaimes et al., 2021, Chen et al., 2022). DTI has reduced validity in regions with crossing fiber populations (Alexander et al., 2001, 2002), which is of particular relevance here as the fetal brain is characterised by incoherent immature axonal bundles, transient cellular structures, and an increased partial volume effect in smaller brains (Jeurissen, 2013). Therefore, to adapt to the unique fetal imaging context, a suitable alternative model was applied to the data, Multi-Shell Multi-Tissue Constrained Spherical Deconvolution (MSMT-CSD). MSMT-CSD utilises multi-shell DWI to deconvolve the diffusion signal into multiple tissue types in the brain (Jeurissen et al., 2014), and in doing so can resolve multiple fiber orientations within a voxel (Tournier et al., 2004). To account for the dynamic contrast changes between tissue types and the inherently low signal to noise ratio, we deconvolve the signal into constituent components: tissue, the "white-matter-like" signal and fluid, or CSF. This is used to produce 'tissue fraction' and 'fluid fraction' maps that convey the contributions from each tissue type to the overall diffusion signal. This model assumes that the white matter response function is anisotropic, whereas the grey matter and CSF response functions are isotropic, and therefore tissue fraction can be considered complementary to FA, and fluid fraction (the reciprocal to tissue fraction) is analogous to MD.

We aligned the surfaces, T2 and DWI volumes for each subject, and used a ±2mm ribbon around the inner cortical plate segmentation boundary to obtain diffusion metrics of the SP (inside boundary) and CP (outside boundary) at each vertex. The 2 mm distance was chosen to match the resolution of the diffusion imaging (2 mm isotropic). Projecting these values to the white matter surface highlighted regionally variant patterns of diffusion metrics across the brain that change with GA (Figure 2). Both FA and tissue fraction appear to have lower values in the central sulcus, higher values in frontal and temporal lobes and regions of asymmetry between left and right hemispheres that change with GA.

To summarise the general trend across the second to third trimester, the mean value for each diffusion metric was calculated across all vertices within the CP and SP and plotted against GA (Figure 2). This analysis highlighted specific maturational trends for each diffusion metric across the surface between 24 and 36 GW, with both the mean fluid fraction and mean MD decreasing with age in the CP and SP (Figure 2b, d). In contrast, FA and tissue fraction showed different trends. FA decreased linearly towards term (Figure 2a), whereas tissue fraction was stable up to 30 GW and then rapidly increased towards

term (Figure 2c). FA values represent the principal eigenvector, representing only the principal direction of diffusion, and are therefore sensitive to the coherent radial alignment of the CP and SP in the youngest fetuses. When the neuropil increases in complexity, and there is a multi-directional microstructural environment, FA decreases. Whereas tissue fraction, which captures the higher angular components of the diffusion signal, increases as the neuropil complexity increases.

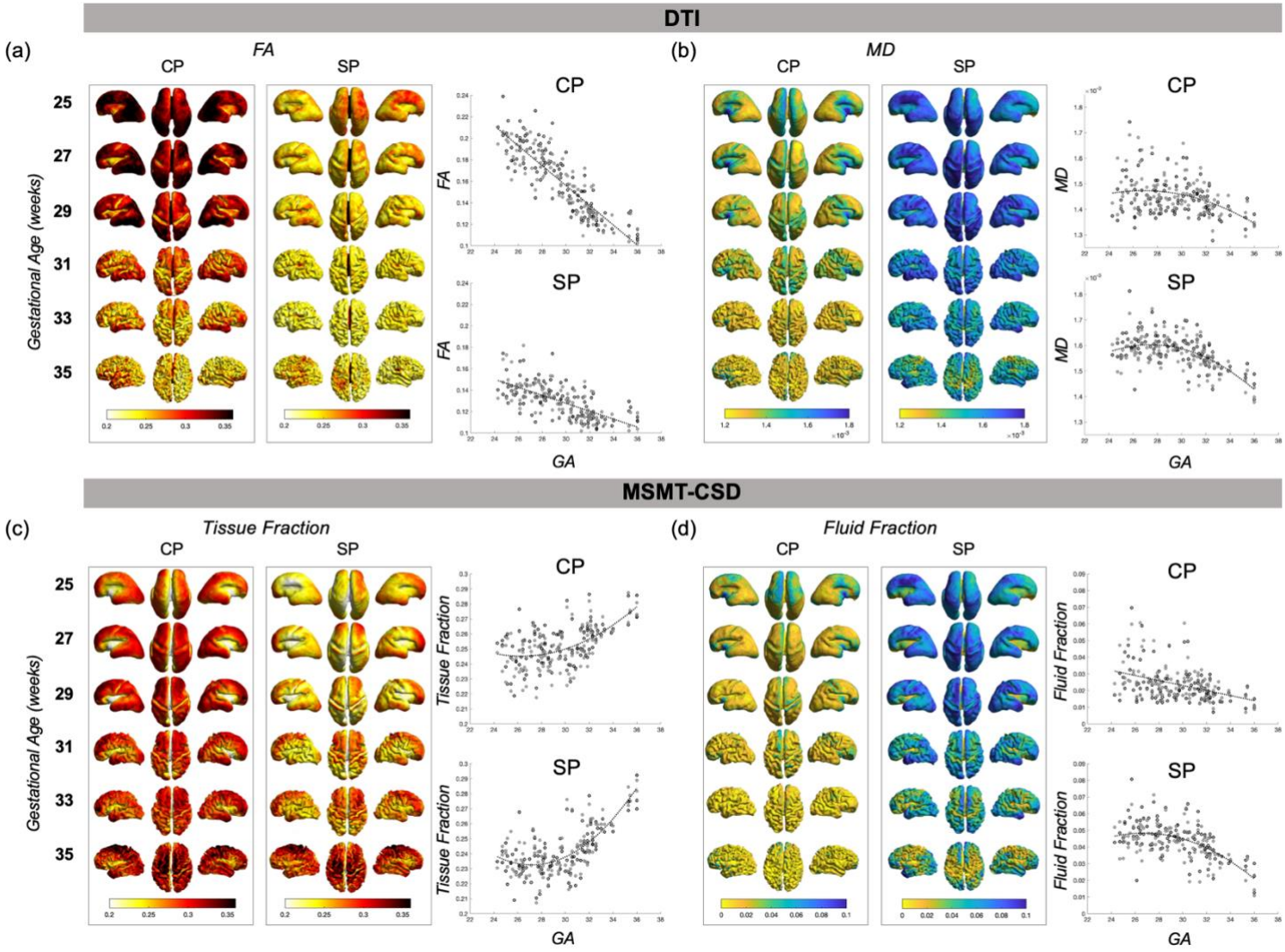

Figure 2. Biweekly mean CP (CP) and SP (SP) microstructure projected to the white matter surface for MSMT-CSD derived metrics (tissue and fluid fraction) and DTI metrics (fractional anisotropy (FA), and mean diffusivity (MD)). Right hand side plots show mean diffusion metrics (grey = left, black = right) across the whole brain in the CP and SP of each subject, charted against the GA of the subject. Certain metrics were best fit with a linear trend, and others using a 2nd order polynomial curve.

Tissue fraction decreases as a function of sulcal depth, independent of age.

To disentangle the effect of age-related maturation and test the hypothesis that microstructural maturation accompanies the formation of cortical folds, we analysed the coupling between cortical folding and diffusion metrics within local areas in individual subjects. We identified patches of cortex by finding neighbours of a central vertex up to 5 degrees of separation (Figure 3a) and calculated the correlation between tissue fraction and sulcal depth in the local area. We then projected the Pearson r value onto the surface to describe this correlation at each vertex across the whole brain (Figure 3b).

In the majority of local neighbourhoods, within-subject CP and SP tissue fraction were negatively associated with sulcal depth, implying that at a global level, tissue fraction progressively decreases in both compartments down the sulcal bank into the sulcal fundus regions. At the level of individual subjects, this relationship was not only present at the onset of gyrification in early emerging sulci, such as central sulcus (27 GW), but also through to the later stages of the third trimester as cortical folds become more mature (Figure 3b). When exploring this relationship across the cohort, subjects were grouped every two weeks to calculate the mean Pearson's correlation coefficient at each vertex. After statistical testing, this association was robust to correction for multiple comparisons using FDR across all vertices and for every biweekly GA group ($q = 0.05$) (Figure 3c). The association was the most prominent in brain regions where sulci were forming, at 25 GW, significant neighbourhood associations were only seen in the sylvian fissure with progression then seen at 27 GW in the central sulcus, and by 35 GW in most primary sulci (Figure 3c).

We then performed a linear regression on the coupling Pearson r values with GA, to explore whether the association between sulcal depth and tissue fraction strengthens with age (Figure 3d), in the SP and CP. We corrected for multiple comparisons using FDR ($q = 0.05$) and projected the significant beta coefficients from the linear regression onto the surface (Figure 3d). There was a significant, negative beta across the surface, implying that the negative correlation between sulcal depth and tissue fraction strengthens with GA. We also observed that the magnitude of beta did not show strong variations between brain regions, suggesting that the association between sulcal depth and tissue fraction strengthens uniformly and proportionally with age in both the SP and CP.

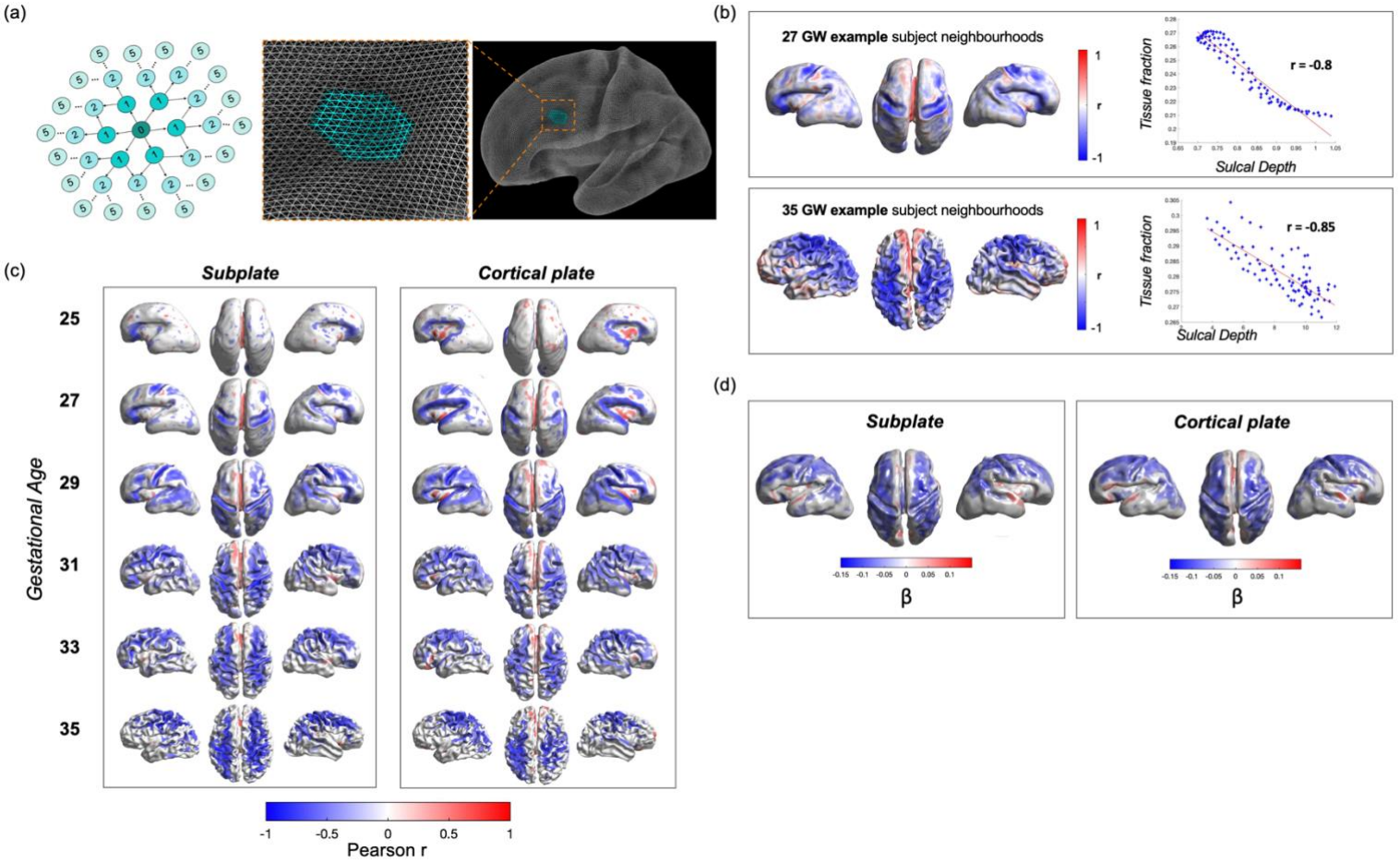

Figure 3. Within-subject tissue fraction vs. sulcal depth neighbourhood analysis (a) Schematic to demonstrate the neighbourhood concept for local patch analysis on the surface, and the degrees of separation between the central vertex and surrounding neighbours (5 degrees). (b) Example of coupling in different aged subjects. Plots show example of how 'r' value is derived, correlating sulcal depth and tissue fraction in local patches, eg. patches in the central sulcus area at 27 GW and 37 GW. (c) Mean Pearson r for subjects grouped into two-weekly bins, representing correlation between tissue fraction and sulcal depth in CP and SP across the whole brain (shown only significant values after FDR correction). (d) Beta coefficients derived from linear regression of Pearson r values against GA, for SP and CP (shown only significant values after FDR correction).

Tissue fraction minima are present in the unfolded brain, in regions that become sulci in the third trimester

To investigate whether changes in microstructure precede the emergence of cortical convolutions, we used the same neighbourhood approach but carried out an age-mismatched analysis (see Methods). Exploiting the conserved spatial configuration of primary cortical folds between individuals, we quantified the coupling between mature sulcal depth values (35 GW average) and tissue fraction in the younger half of the cohort (25 GW – 30 GW). This age-mismatched analysis (Figure 4) highlighted

microstructural variations across a sulcal area prior to presence of a fold, revealing numerous brain regions across the surface where tissue fraction in unfolded regions in younger subjects correlated with future sulcal depth values (Figure 4a,b). Significant trends were identified in different major sulcal landmarks, including the inferior frontal sulcus, superior temporal sulcus and post-central sulcus (indicated with arrows), where significant coupling was not shown in the *age-matched* analysis.

To explore this relationship in more detail, we zoomed in on specific sulcal regions of interest (ROIs) in each gestational week (Figure 4c). In the central sulcus, at 25 GW there was marked variability between subjects and thus when averaging within this group there was no consistent corelation between between tissue fraction and future depth (Figure 4c(i)). However, by 26 GW a negative relationship (blue) was evident at more vertices which is then consistently seen from 27 GW onwards across the central sulcus. Asymmetries were also noted between left and right hemispheres, particularly in the youngest subjects. In the other sulcal ROIs, including the inferior temporal sulcus, post central sulcus and superior temporal sulcus, the correlation values were consistent both spatially, across the sulcus, and temporally, across GA from 25 to 30 GW (Figure 4c(ii),(iii),(iv)).

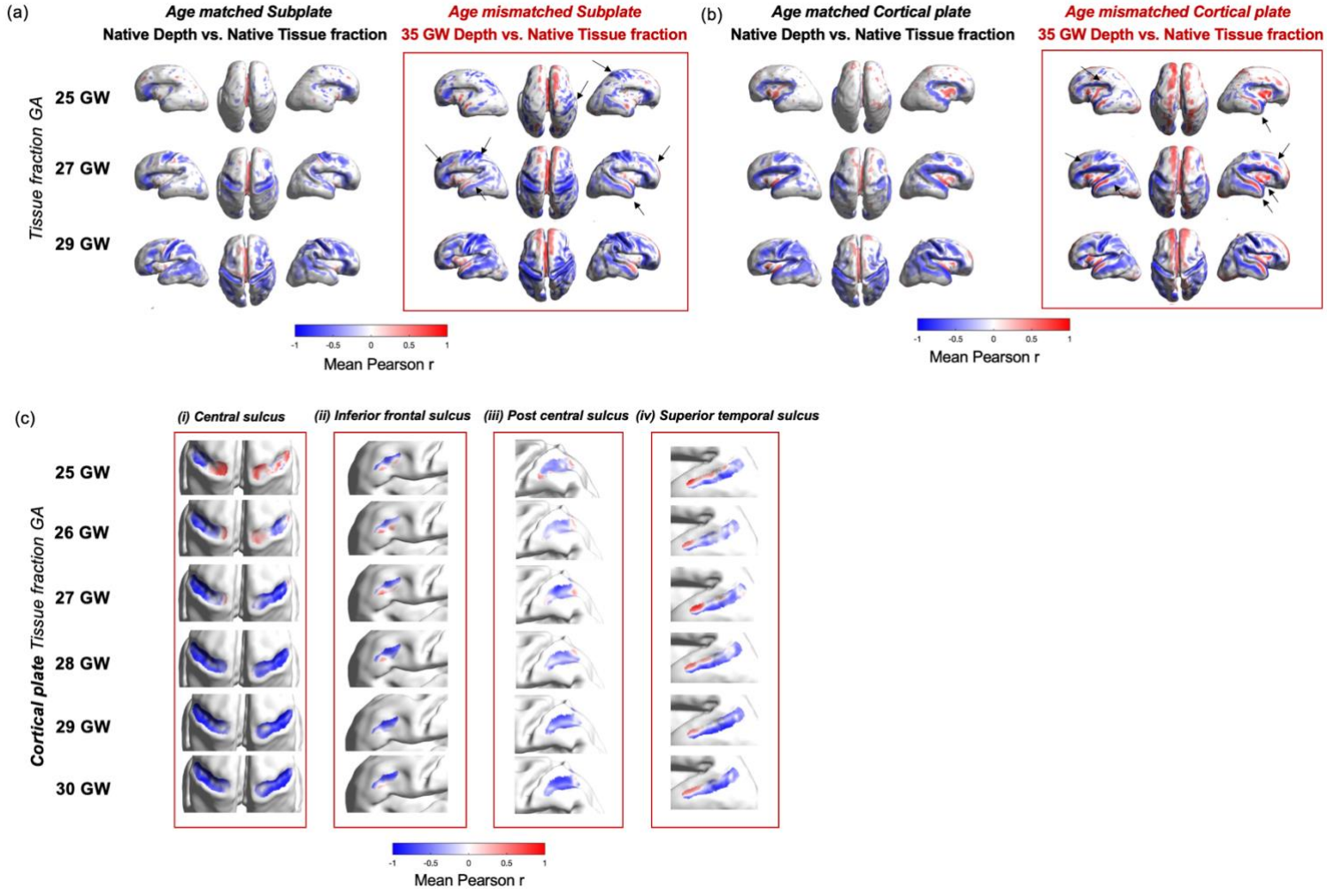

Figure 4. Age-mismatched analysis highlights brain regions where changes in microstructure precede the formation of sulcal folds, in the (a) SP and (b) CP. Red boxes are whole-brain mean Pearson r correlation coefficient values for the correlation between mature 35 GW average sulcal depth values and native individual subject tissue fraction. Arrows indicate areas of strong change between age matched and mismatched analysis, including the inferior frontal sulcus, superior temporal sulcus, post-central sulcus and insula. (c) Close-up, of specific primary sulci using CP tissue fraction values, projected onto 27 GW surface, including (i) Central Sulcus, (ii) Inferior Frontal Sulcus (iii) Post central sulcus and (iv) Superior temporal sulcus.

Discussion

In this study, we investigate how the microstructure of transient compartments in the fetal brain transitions at the onset of the cortical folding process in the human brain in vivo. Specialised acquisition and image reconstruction techniques were designed to overcome the unique challenges associated with the in utero environment, such as artefacts due to fetal head motion and geometric distortion due to magnetic inhomogeneities (Christiaens et al., 2021). These methods significantly enhanced data quality, enabling more reliable and accurate imaging analysis. With this unique multi-shell fetal HARDI dataset, it was possible to explore the relationship between the developmental processes that influence the cytoarchitecture of the SP and CP, and the macrostructural appearance of sulci and gyri. We found regionally heterogenous patterns of cortical microstructural and macrostructural development with GA, and a robust brain-wide inverse relationship between tissue fraction and sulcal depth. We then establish that this local reduction in tissue fraction precedes the emergence of cortical folds later in gestation, supporting previous hypotheses that regional variations in cellular morphological maturation in both the SP and CP contribute to the intracortical forces that drive cortical folding (Wang et al., 2017, Del Toro et al., 2017).

The microstructure of the SP and CP matures over the same timeframe that primary and secondary cortical folds emerge (Huang et al., 2014, McKinstry et al., 2002, Ball et al., 2013, Batalle et al., 2019), however the precise relationship between them has not been established. Tissue fraction and FA can be considered complementary metrics for describing anisotropic, coherently aligned tissue-like signal and microstructural maturity. However, in the fetal brain, we observed opposite trends between the whole-brain average FA and tissue fraction metrics in the CP and SP, reflecting the different developmental processes captured by these metrics, as they quantify different components of the diffusion signal.

There are a multitude of biological processes occurring simultaneously in the CP and SP in the third trimester which create a complex microstructural environment. These include the disappearance of radial glial scaffolding, appearance of immature oligodendrocytes, dendritic arborization and axonal

branching. We recapitulate ex-utero observations, identifying a decrease in whole-brain FA in both the CP and SP, with a higher rate of change in the CP. This reflects a loss of radial coherence in the CP, the disassembly of radial scaffolding in the SP (as neuronal migration finishes at the end of the second trimester) and the isotropic restriction of water movement as dendritic arborization occurs (Wang et al., 2017, Dean et al., 2013, Sizonenko et al., 2007). We also observe MD decreases, as synaptic density, cellular and organelle density increases (Dean et al., 2013, Sizonenko et al., 2007). These trends in DTI metrics have been observed in preterm infants over a comparable timeframe in early development (McKinstry et al., 2002, Vinall et al., 2013, Ball et al., 2013, Batalle et al., 2019), and in post-mortem tissue from other gyrencephalic mammals such as ferrets and macaques (Kroenke et al., 2007, 2009; Yu et al., 2016).

The MSMT-CSD decomposition of the diffusion MRI signal into tissue and fluid components overcomes some crossing fiber related limitations of DTI methods, allowing quantification of maturing axonal and dendritic morphology (Alexander et al., 2002, Tournier 2010). We observe tissue fraction increases with GA over the third trimester, that reflect maturing neuronal morphology and reductions in extracellular water, as dendritic trees develop and thalamocortical fibres synapse in the CP and SP (Kostovic 2010). Tissue fraction increases linearly in the CP, whereas in the SP a rapid increase is not seen until after 30 GW (Figure 3). This difference in maturational trend between compartments highlights the sensitivity of MSMT-CSD to the maturation of neuronal morphology, and the increasing neuropil complexity as immature oligodendrocytes begin extending their processes and commencing pre-myelination, at approximately 30 GW in SP regions (Back et al., 2002, Kostovic & Judas 2010). Thus, applying multiple modelling methods exploits the information in the multi-shell diffusion data, and enables improved characterisation of the biological complexity, which was not previously possible with in utero imaging.

To investigate if the heterogeneous microstructural maturation in different cortical regions plays a mechanistic role in cortical folding, we quantified the relationship or ‘coupling’ between SP/CP microstructure and sulcal depth. To disentangle the effect of GA, we calculated correlations within local neighbourhoods at the individual subject level and found a significant brain-wide relationship in all subjects, showing sulcal depth is inversely correlated with tissue fraction. We observe these local reductions in tissue fraction in the deepest parts of sulci at the onset of cortical folding (in the sylvian fissure at 25 GW and in the central sulcus at 27 GW). This trend emerges across the cortex as more regions fold, persisting throughout the cohort up to 35 GW as sulci deepen and mature. The higher tissue fractions we observe in gyral crowns are supported by previous studies across multiple gyrencephalic species, identifying higher myelinated fibre density, greater vertical alignment of pyramidal neurons, and longer more elaborate dendritic trees in gyral crowns than in sulcal fundi (Nie et al., 2012, Mortazavi et al 2017, Llinares-Benadero and Borrell, 2019). Our result also recapitulates

ex vivo observations describing a greater density of fibre bundles and persistence of radial pathways in developing gyral areas compared to sulcal areas (Takahashi et al., 2012). Overall, our analysis reveals that the neuroanatomical differences between gyral and sulcal areas observed in adulthood are already present at the formation of the folds in utero, suggesting this conformational difference in microstructure has mechanistic importance.

We examined whether microstructural changes predate macrostructure by using an age-mismatched coupling analysis to test the hypothesis that local minima in tissue fraction precedes the formation of cortical folds. We correlated native tissue fraction values in the youngest subjects with unfolded brain regions (25 GW – 29 GW) with 35 GW group-average sulcal depth values, back-projecting a map of folded brain regions onto the unfolded brain (Figure 4). We identified significant negative correlations between future sulcal depth and tissue fraction values across unfolded brain regions in the youngest subjects. With this analysis, we reveal dynamic changes in CP and SP microstructure which occur immediately prior to the formation of cortical convolutions, suggesting that the developmental processes captured by the diffusion signal in these regions initiate the buckling of the cortex to drive folding.

The late second to third trimester is characterised by synaptogenesis, increasing maturation of dendritic and axonal arbours, extending glial processes, and generally increasing complexity of the neuropil (Kostovic 2005, Wilson et al., 2023). The decreased tissue fraction in regions that are about to fold suggests that the regional variation in the density and complexity of neuropil in the CP and SP plays a mechanistic function in the onset of folding across the brain. Variations in the density and morphology of neurons accumulating in the CP have been observed in previous work and are thought to be driven in part by differential patterning of gene expression in the outer subventricular zone (OSVZ) and ventricular zone (VZ), which also reliably map the prospective location of sulcal and gyral folds (Welker 1990, Kostovic 1990, Llinares-Benadero & Borrell, 2019). Recently published work has explored this at the histological level in primates, and suggested that cortical expansion and subsequent gyrification are driven by rapid, post-neurogenic neuropil growth, addition of glial cells, and expansion of large white matter tracts (Shinmyo et al., 2022, Rash et al., 2023).

In summary, when placed in the context of previous work, our observations in the fetal brain support the hypotheses that regional variations in neurogenesis and the dispersion of migrating neurons lead to different initial densities of accumulated neurons in the CP before folding. This is accompanied by regional differences in morphological expansion of dendritic and axonal arbors, and in cortical tangential growth, which combine and culminate in a specific sulcal folding pattern. Overall, this study supports the theory that the formation of the primary sulci is under close genetic control (Im & Grant 2019) and suggests an important role of neuronal and glial cellular morphological maturation, producing

intracortical forces to drive the formation of primary folds (Richman et al., 1975, Wang et al. 2017, Llinares-Benadero & Borrell 2019).

Conclusion

Using advanced in utero imaging techniques, we quantify the direct role of transient compartments in the formation of cortical convolutions. We show that cytoarchitectural differences between gyral and sulcal regions, previously observed in adults and non-human primates, are already present in utero at the onset of gyrification. Moreover, we find local minima in tissue fraction across the cortex which precede the formation of primary cortical folds, highlighting the predictive power of dynamic changes in the diffusion MR signal to anticipate the emergence of macrostructure. In this analysis, we uncover a direct link between micro and macrostructure that offers mechanistic insight about how gyrification begins in the fetal brain, with clear implications for understanding how folding abnormalities arise in utero.

Methods

Acquisition and pre-processing

112 in utero fetal T2 and diffusion MRI datasets (see Supplementary for cohort information) were acquired on a Philips Achieva 3T system with a 32-channel cardiac coil (Price et al., 2019). T2 acquisition involved multiple single-shot turbo spin echo sequences with TE = 250ms, TR = 2265ms (Price et al., 2019). DWI was acquired with a combined spin and field echo (SAFE) sequence at 2 mm isotropic resolution and multi-shell high angular resolution diffusion encoding (15 volumes at b=0s/mm², 46 volumes at b=400s/mm², and 80 volumes at b=1000s/mm²) (Christiaens et al., 2019). T2 datasets were reconstructed to 0.5 mm isotropic resolution using an automated bespoke pipeline (Cordero-Grande et al., 2019). HARDI datasets were reconstructed to 0.8 mm, using a data driven representation of the spherical harmonics and radial decomposition (SHARD). The SHARD pipeline caters to the motion corrupted fetal data, using dynamic distortion correction and slice-to-volume motion correction framework (Cordero-Grande et al., 2019, Christiaens et al., 2021). Information about the quality control can be found in the Supplementary material.

Tissue segmentation & image registration

Cortex, white matter and CSF probability maps were generated using the 'Brain vOlumetry and aUtomated parcellatioN for 3D feTal MRI' (BOUNTI) tool (Uus et al., 2023), an automated deep learning brain tissue parcellation pipeline trained using the dHCP fetal cohort.

To align individual subject diffusion and T2w volumes, we used FLIRT boundary-based registration in FSL (Jenkinson et al., 2001, Jenkinson et al., 2012).

To align individual subject T2w volumes to a common space, a spatiotemporal atlas of the fetal brain was used (https://gin.g-node.org/kcl_cdb/fetal_brain_mri_atlas) (Uus et al., 2023), constructed using the Medical Image Registration ToolKit (MIRTK) atlas generation pipeline (Schuh et al., 2018) (https://biomedia.doc.ic.ac.uk/software/mirtk/). For each subject, multi-channel ANTs non-linear symmetric diffeomorphic image registration was used (Avants et al., 2008), with a combination of the T2w volume and the cortex probability map as inputs. In this way, we created warps between native T2 space and age-matched weeks of the atlas. The multi-channel approach improved accuracy at cortical boundaries, particularly in the oldest subjects.

Surface reconstruction, registration, and vertex correspondence

To extract hemispheric surfaces on the inner cortical plate boundary, we applied the marching-cube algorithm in CIVET-2.1.0 software package (Lepage et al., 2021; Liu et al., 2021). Inner parts of the segmented CP were binarized and the initial meshes were tessellated by fitting the boundary of the inner part of CP. We resampled the initial meshes to the standard format surfaces containing 81,920 triangles and 40,962 vertices (Lepage et al., 2021; Liu et al., 2021). To eliminate small geometrical noise, Taubin smoothing was applied to the surfaces (Taubin, 1995). Then, the surfaces were registered to a 28 GW template surface (Serag et al., 2012; Yun et al., 2019) to guarantee the vertex correspondence among individual surfaces. We used a 2D sphere-to-sphere warping method, which searches optimal correspondence of vertices based on folding similarity between individual and template surfaces (Robbins et al., 2004; Boucher et al., 2009).

Surface metric calculation

Three metrics describing surface features were chosen for this study, mean curvature, surface area and sulcal depth. The mean curvature and surface area were computed according to the angular deviation from a patch around each vertex on the surface model and the Voronoi region around each vertex on the cortical surface (Meyer et al., 2003). Sulcal depth was calculated using the adaptive distance transform (ADT) method (Yun et al. 2013).

Diffusion modelling: using DTI and MSMT-CSD to derive maps of diffusion metrics.

Two different approaches to modelling the DWI signal were used, the traditional diffusion tensor method (DTI) (Basser et al., 1994) and multi-shell multi-tissue constrained spherical deconvolution (MSMT-CSD) (Jeurissen et al., 2014). The diffusion tensor was estimated from the b=0 and b=1000 volumes for each subject, using the iteratively reweighted linear least squares estimator in MRtrix3 (Tournier 2019). Subsequently FA/MD maps were calculated from the tensor (Basser et al., 1994).

For MSMT-CSD derived metrics, in each subject, white matter response functions were extracted from areas of relatively mature white matter (corticospinal tract and corpus callosum) using the Tournier algorithm (Tournier et al., 2019; Tournier et al., 2013). CSF responses were extracted using masks of the ventricles using the Dhollander algorithm in MRtrix3 (Jeurissen et al., 2014; Tournier et al., 2019; Tournier et al., 2013). To obtain group-average response functions, the white matter response functions of the oldest 20 subjects were averaged (approximating relatively mature fetal white matter) and the CSF group-average response function was calculated from the whole cohort. Using these two average response functions, the dMRI signal of all subjects was subsequently decomposed into a tissue and fluid component, using the tournier algorithm applied via the MRtrix3 software package (Tournier 2019), and resulting components were intensity normalised for each subject (Raffelt et al., 2011). The tissue and fluid component maps were normalised to 1, for ease of interpretation, then labelled as tissue and fluid 'fraction'.

Projecting from the surface boundary into diffusion maps

The inverse transform was applied to the surfaces to register them back to native T2 space, and surface coordinates were converted to cartesian space (x,y,z). This preserved the vertex correspondence between all subjects and the 28 GW surface template, such that the surface normal could be used to extrapolate from the white matter boundary into the T2-aligned diffusion maps at equivalent points across the surface. To obtain estimates of microstructure in the SP and CP, we projected ±2mm (twice the surface normal) inside (SP) and outside (CP) the white matter boundary, interpolating into volumetric space to create a ribbon of voxels that was used to sample the maps of diffusion metrics.

1. Fractional Anisotropy (FA) (DTI)
2. Mean Diffusivity (MD) (DTI)
3. Tissue Fraction (MSMT-CSD)
4. Fluid Fraction (MSMT-CSD)

Coupling analysis within-subject

To understand the local relationships within cortical areas of individual subjects, correlation analysis was performed within vertex neighbourhoods, to calculate the 'coupling' between microstructure and macrostructure (adapted from Vandekar et al., 2016). Custom-built MATLAB analysis pipelines were written, to find neighbours around a central vertex up to 5 degrees of separation on the surface mesh. Then the Pearson correlation coefficient (r) and corresponding p value was calculated to describe the relationship between diffusion and surface metrics in each neighbourhood. The subjects were grouped into bi-weekly bins, and a single sample t-test was used on the Pearson r values at each vertex, within each age group, to identify significant vertices. To correct for multiple comparisons across all vertices, we controlled for the false discovery rate (FDR) (Benjamini & Hochberg 1995), to identify significant features while incurring a relatively low proportion of false positives. The mean r value is displayed at the vertices which survived FDR correction in each age bin (23, 25, 27.. 35 GW).

Age-mismatched coupling analysis

Using surface registration and vertex correspondence across the whole brain it was possible to project a map of folded brain regions (mean sulcal depth 35 GW) onto the unfolded brain (25 GW – 29 GW). The same technique of analysing coupling in local patches was repeated, but instead of correlating native sulcal depth and diffusion metrics, the average sulcal depth values at 35 GW were correlated with native diffusion metrics (FA, MD, tissue and fluid fraction). To display the results across the whole cohort, the r values were averaged between subjects in biweekly bins. Statistical testing for significant correlations was repeated as above, correcting for FDR across all vertices, then displaying significant r values.

References

Aggarwal, M., Gobius, I., Richards, L.J., Mori, S., 2015. Diffusion MR Microscopy of Cortical Development in the Mouse Embryo. Cerebral Cortex 25, 1970–1980. https://doi.org/10.1093/cercor/bhu006

Alexander, D.C., Barker, G.J., Arridge, S.R., 2002. Detection and modeling of non-Gaussian apparent diffusion coefficient profiles in human brain data. Magn. Reson. Med. 48, 331–340. https://doi.org/10.1002/mrm.10209

Ball, G., Srinivasan, L., Aljabar, P., Counsell, S.J., Durighel, G., Hajnal, J.V., Rutherford, M.A., Edwards, A.D., 2013. Development of cortical microstructure in the preterm human brain. Proc. Natl. Acad. Sci. U.S.A. 110, 9541–9546. https://doi.org/10.1073/pnas.1301652110

Barkovich, A.J., Guerrini, R., Kuzniecky, R.I., Jackson, G.D., Dobyns, W.B., 2012. A developmental and genetic classification for malformations of cortical development: update 2012. Brain 135, 1348–1369. https://doi.org/10.1093/brain/aws019

Batalle, D., O'Muircheartaigh, J., Makropoulos, A., Kelly, C.J., Dimitrova, R., Hughes, E.J., Hajnal, J.V., Zhang, H., Alexander, D.C., Edwards, A.D., Counsell, S.J., 2019. Different patterns of cortical maturation before and after 38 weeks gestational age demonstrated by diffusion MRI in vivo. NeuroImage 185, 764–775. https://doi.org/10.1016/j.neuroimage.2018.05.046

Cachia, A., Roell, M., Mangin, J.-F., Sun, Z.Y., Jobert, A., Braga, L., Houde, O., Dehaene, S., Borst, G., 2018. How interindividual differences in brain anatomy shape reading accuracy. Brain Struct Funct 223, 701–712. https://doi.org/10.1007/s00429-017-1516-x

Chen, R., Sun, C., Liu, T., Liao, Y., Wang, J., Sun, Y., Zhang, Y., Wang, G., Wu, D., 2022. Deciphering the developmental order and microstructural patterns of early white matter pathways in a diffusion MRI based fetal brain atlas. NeuroImage 264, 119700. https://doi.org/10.1016/j.neuroimage.2022.119700

Chi, J.G., Dooling, E.C., Gilles, F.H., 1977. Gyral development of the human brain. Ann Neurol. 1, 86–93. https://doi.org/10.1002/ana.410010109

Christiaens, D., Cordero-Grande, L., Pietsch, M., Hutter, J., Price, A.N., Hughes, E.J., Vecchiato, K., Deprez, M., Edwards, A.D., Hajnal, J.V., Tournier, J.-D., 2021. Scattered slice SHARD reconstruction for motion correction in multi-shell diffusion MRI. NeuroImage 225, 117437. https://doi.org/10.1016/j.neuroimage.2020.117437

Christiaens, D., Slator, P.J., Cordero-Grande, L., Price, A.N., Deprez, M., Alexander, D.C., Rutherford, M., Hajnal, J.V., Hutter, J., 2019. In Utero Diffusion MRI: Challenges, Advances, and Applications. Topics in Magnetic Resonance Imaging 28, 255–264. https://doi.org/10.1097/RMR.0000000000000211

Cordero-Grande, L., Price, A.N., Ferrazzi, G., Hutter , J., Christiaens, D., Hughes E., Hajnal J. V., 2018. Spin And Field Echo (SAFE) dynamic field correction in 3T fetal EPI. Joint Annual Meeting ISMRM-ESMRMB.

Cordero-Grande, L., Christiaens, D., Hutter , J., Price, A.N., Hajnal, J.V., 2019. Complex diffusion-weighted image estimation via matrix recovery under general noise models NeuroImage 200:391–404. https://doi.org/10.1016/j.neuroimage.2019.06.039

Finlay, B.L., Darlington, R.B., 1995. Linked Regularities in the Development and Evolution of Mammalian Brains. Science 268, 1578–1584. https://doi.org/10.1126/science.7777856

Dean, J.M., McClendon, E., Hansen, K., Azimi-Zonooz, A., Chen, K., Riddle, A., Gong, X., Sharifnia, E., Hagen, M., Ahmad, T., Leigland, L.A., Hohimer, A.R., Kroenke, C.D., Back, S.A., 2013. Prenatal Cerebral Ischemia Disrupts MRI-Defined Cortical Microstructure Through Disturbances in Neuronal Arborization. Sci. Transl. Med. 5. https://doi.org/10.1126/scitranslmed.3004669

Deng, F., Jiang, X., Zhu, D., Zhang, T., Li, K., Guo, L., Liu, T., 2014. A functional model of cortical gyri and sulci. Brain Struct Funct 219, 1473–1491. https://doi.org/10.1007/s00429-013-0581-z

Dudink, J., Buijs, J., Govaert, P., Van Zwol, A.L., Conneman, N., Van Goudoever, J.B., Lequin, M., 2010. Diffusion tensor imaging of the CP and SP in very-low-birth-weight infants. Pediatr Radiol 40, 1397–1404. https://doi.org/10.1007/s00247-010-1638-2

Fernández, V., Llinares-Benadero, C., Borrell, V., 2016. Cerebral cortex expansion and folding: what have we learned? EMBO J 35, 1021–1044. https://doi.org/10.15252/embj.201593701

Fischl, B., Dale, A.M., 2000. Measuring the thickness of the human cerebral cortex from magnetic resonance images. Proc. Natl. Acad. Sci. U.S.A. 97, 11050–11055. https://doi.org/10.1073/pnas.200033797

Goldman, P.S., Galkin, T.W., 1978. Prenatal removal of frontal association cortex in the fetal rhesus monkey: Anatomical and functional consequences in postnatal life. Brain Research 152, 451–485. https://doi.org/10.1016/0006-8993(78)91103-4

Goldman-Rakic, P.S., 1980. Morphological consequences of prenatal injury to the primate brain. Prog Brain Res 53, 1–19.

Hilgetag, C.C., Barbas, H., 2005. Developmental mechanics of the primate cerebral cortex. Anat Embryol 210, 411–417. https://doi.org/10.1007/s00429-005-0041-5

Hogstrom, L.J., Westlye, L.T., Walhovd, K.B., Fjell, A.M., 2013. The Structure of the Cerebral Cortex Across Adult Life: Age-Related Patterns of Surface Area, Thickness, and Gyrification. Cerebral Cortex 23, 2521–2530. https://doi.org/10.1093/cercor/bhs231

Huang, H., Vasung, L., 2014. Gaining insight of fetal brain development with diffusion MRI and histology. Int. J. Dev. Neurosci 32, 11–22. https://doi.org/10.1016/j.ijdevneu.2013.06.005

Huang, H., Xue, R., Zhang, J., Ren, T., Richards, L.J., Yarowsky, P., Miller, M.I., Mori, S., 2009. Anatomical Characterization of Human Fetal Brain Development with Diffusion Tensor Magnetic Resonance Imaging. J. Neurosci. 29, 4263–4273. https://doi.org/10.1523/JNEUROSCI.2769-08.2009

Im, K., Grant, P.E., 2019. Sulcal pits and patterns in developing human brains. NeuroImage 185, 881–890. https://doi.org/10.1016/j.neuroimage.2018.03.057

Im, K., Jo, H.J., Mangin, J.-F., Evans, A.C., Kim, S.I., Lee, J.-M., 2010. Spatial Distribution of Deep Sulcal Landmarks and Hemispherical Asymmetry on the Cortical Surface. Cerebral Cortex 20, 602–611. https://doi.org/10.1093/cercor/bhp127

Jaimes, C., Machado-Rivas, F., Afacan, O., Khan, S., Marami, B., Ortinau, C.M., Rollins, C.K., Velasco-Annis, C., Warfield, S.K., Gholipour, A., 2020. In vivo characterization of emerging white matter microstructure in the fetal brain in the third trimester. Hum Brain Mapp 41, 3177–3185. https://doi.org/10.1002/hbm.25006

Kostović, I., Jovanov-Milošević, N., Radoš, Milan, Sedmak, G., Benjak, V., Kostović-Srzentić, M., Vasung, L., Čuljat, M., Radoš, Marko, Hüppi, P., Judaš, M., 2014. Perinatal and early postnatal reorganization of the SP and related cellular compartments in the human cerebral wall as revealed by histological and MRI approaches. Brain Struct Funct 219, 231–253. https://doi.org/10.1007/s00429-012-0496-0

Kostović, I., Judaš, M., 2010. The development of the SP and thalamocortical connections in the human foetal brain: Human foetal cortical circuitry. Acta Paediatrica 99, 1119–1127. https://doi.org/10.1111/j.1651-2227.2010.01811.x

Kriegstein, A., Noctor, S., Martínez-Cerdeño, V., 2006. Patterns of neural stem and progenitor cell division may underlie evolutionary cortical expansion. Nat Rev Neurosci 7, 883–890. https://doi.org/10.1038/nrn2008

Kroenke, C.D., Taber, E.N., Leigland, L.A., Knutsen, A.K., Bayly, P.V., 2009. Regional Patterns of Cerebral Cortical Differentiation Determined by Diffusion Tensor MRI. Cerebral Cortex 19, 2916–2929. https://doi.org/10.1093/cercor/bhp061

Kroenke, C.D., Van Essen, D.C., Inder, T.E., Rees, S., Bretthorst, G.L., Neil, J.J., 2007. Microstructural Changes of the Baboon Cerebral Cortex during Gestational Development Reflected in Magnetic Resonance Imaging Diffusion Anisotropy. J. Neurosci. 27, 12506–12515. https://doi.org/10.1523/JNEUROSCI.3063-07.2007

Lefèvre, J., Mangin, J.-F., 2010. A Reaction-Diffusion Model of Human Brain Development. PLoS Comput Biol 6, e1000749. https://doi.org/10.1371/journal.pcbi.1000749

Llinares-Benadero, C., Borrell, V., 2019a. Deconstructing cortical folding: genetic, cellular and mechanical determinants. Nat Rev Neurosci 20, 161–176. https://doi.org/10.1038/s41583-018-0112-2

Lohmann, G., Von Cramon, D.Y., Colchester, A.C.F., 2008. Deep Sulcal Landmarks Provide an Organizing Framework for Human Cortical Folding. Cerebral Cortex 18, 1415–1420. https://doi.org/10.1093/cercor/bhm174

McKinstry, R.C., 2002. Radial Organization of Developing Preterm Human Cerebral Cortex Revealed by Non-invasive Water Diffusion Anisotropy MRI. Cerebral Cortex 12, 1237–1243. https://doi.org/10.1093/cercor/12.12.1237

Mortazavi, F., Romano, S.E., Rosene, D.L., Rockland, K.S., 2017. A Survey of White Matter Neurons at the Gyral Crowns and Sulcal Depths in the Rhesus Monkey. Front. Neuroanat. 11, 69. https://doi.org/10.3389/fnana.2017.00069

Mota, B., Herculano-Houzel, S., 2015. Cortical folding scales universally with surface area and thickness, not number of neurons. Science 349, 74–77. https://doi.org/10.1126/science.aaa9101

Nie, J., Guo, L., Li, K., Wang, Y., Chen, G., Li, L., Chen, H., Deng, F., Jiang, X., Zhang, T., Huang, L., Faraco, C., Zhang, D., Guo, C., Yap, P.-T., Hu, Xintao, Li, G., Lv, J., Yuan, Y., Zhu, D., Han, J., Sabatinelli, D., Zhao, Q., Miller, L.S., Xu, B., Shen, P., Platt, S., Shen, D., Hu, Xiaoping, Liu, T., 2012. Axonal Fiber Terminations Concentrate on Gyri. Cerebral Cortex 22, 2831–2839. https://doi.org/10.1093/cercor/bhr361

Nordahl, C.W., Dierker, D., Mostafavi, I., Schumann, C.M., Rivera, S.M., Amaral, D.G., Van Essen, D.C., 2007. Cortical Folding Abnormalities in Autism Revealed by Surface-Based Morphometry. J. Neurosci. 27, 11725–11735. https://doi.org/10.1523/JNEUROSCI.0777-07.2007

Price, A., Cordero-Grande, L., Hughes, E., Rutherford, M., Edwards, A. D., & Hajnal, J. V. (2019). The Developing Human Connectome Project (dHCP): Fetal Acquisition Protocol. ISMRM.

Raffelt, D., Tournier, J.-D., Fripp, J., Crozier, S., Connelly, A., Salvado, O., 2011. Symmetric diffeomorphic registration of fibre orientation distributions. Neuroimage 56, 1171–1180. https://doi.org/10.1016/j.neuroimage.2011.02.014

Rakic, P., 2003. Elusive radial glial cells: Historical and evolutionary perspective. Glia 43, 19–32. https://doi.org/10.1002/glia.10244

Rakic, P., 1988. Specification of Cerebral Cortical Areas. Science 241, 170–176. https://doi.org/10.1126/science.3291116

Rana, S., Shishegar, R., Quezada, S., Johnston, L., Walker, D.W., Tolcos, M., 2019. The SP: A Potential Driver of Cortical Folding? Cerebral Cortex 29, 4697–4708. https://doi.org/10.1093/cercor/bhz003

Rash, B.G., Arellano, J.I., Duque, A., Rakic, P., 2023. Role of intracortical neuropil growth in the gyrification of the primate cerebral cortex. Proc. Natl. Acad. Sci. U.S.A. 120, e2210967120. https://doi.org/10.1073/pnas.2210967120

Richman, D.P., Stewart, R.M., Hutchinson, J., Caviness, V.S., 1975. Mechanical Model of Brain Convolutional Development: Pathologic and experimental data suggest a model based on differential growth within the cerebral cortex. Science 189, 18–21. https://doi.org/10.1126/science.1135626

Sizonenko, S.V., Camm, E.J., Garbow, J.R., Maier, S.E., Inder, T.E., Williams, C.E., Neil, J.J., Huppi, P.S., 2007. Developmental Changes and Injury Induced Disruption of the Radial Organization of the Cortex in the Immature Rat Brain Revealed by In Vivo Diffusion Tensor MRI. Cerebral Cortex 17, 2609–2617. https://doi.org/10.1093/cercor/bhl168

Smart, I.H., McSherry, G.M., 1986. Gyrus formation in the cerebral cortex of the ferret. II. Description of the internal histological changes. J Anat 147, 27–43.

Subramanian, L., Calcagnotto, M.E., Paredes, M.F., 2020. Cortical Malformations: Lessons in Human Brain Development. Front. Cell. Neurosci. 13, 576. https://doi.org/10.3389/fncel.2019.00576

Takahashi, E., Folkerth, R.D., Galaburda, A.M., Grant, P.E., 2012. Emerging Cerebral Connectivity in the Human Fetal Brain: An MR Tractography Study. Cerebral Cortex 22, 455–464. https://doi.org/10.1093/cercor/bhr126

Tallinen, T., Chung, J.Y., Biggins, J.S., Mahadevan, L., 2014. Gyrification from constrained cortical expansion. Proc. Natl. Acad. Sci. U.S.A. 111, 12667–12672. https://doi.org/10.1073/pnas.1406015111

Tallinen, T., Chung, J.Y., Rousseau, F., Girard, N., Lefèvre, J., Mahadevan, L., 2016. On the growth and form of cortical convolutions. Nature Phys 12, 588–593. https://doi.org/10.1038/nphys3632

Tournier, J.-D., 2010. The Biophysics of Crossing Fibers, in: Jones, PhD, D.K. (Ed.), Diffusion MRI. Oxford University Press, pp. 465–482. https://doi.org/10.1093/med/9780195369779.003.0028

Tournier, J.-D., Smith, R., Raffelt, D., Tabbara, R., Dhollander, T., Pietsch, M., Christiaens, D., Jeurissen, B., Yeh, C.-H., Connelly, A., 2019. MRtrix3: A fast, flexible and open software framework

for medical image processing and visualisation. NeuroImage 202, 116137. https://doi.org/10.1016/j.neuroimage.2019.116137

Uus, A.U., Kyriakopoulou, V., Makropoulos, A., Fukami-Gartner, A., Cromb, D., Davidson, A., Cordero-Grande, L., Price, A.N., Grigorescu, I., Williams, L.Z.J., Robinson, E.C., Lloyd, D., Pushparajah, K., Story, L., Hutter, J., Counsell, S.J., Edwards, A.D., Rutherford, M.A., Hajnal, J.V., Deprez, M., 2023. BOUNTI: Brain vOlumetry and aUtomated parcellatioN for 3D feTal MRI (preprint). Neuroscience. https://doi.org/10.1101/2023.04.18.537347

Van Essen, D.C., 1997. A tension-based theory of morphogenesis and compact wiring in the central nervous system. Nature 385, 313–318. https://doi.org/10.1038/385313a0

Van Essen, D.C., 2020. A 2020 view of tension-based cortical morphogenesis. Proc. Natl. Acad. Sci. U.S.A. 117, 32868–32879. https://doi.org/10.1073/pnas.2016830117

Vinall, J., Grunau, R.E., Brant, R., Chau, V., Poskitt, K.J., Synnes, A.R., Miller, S.P., 2013. Slower Postnatal Growth Is Associated with Delayed Cerebral Cortical Maturation in Preterm Newborns. Sci. Transl. Med. 5. https://doi.org/10.1126/scitranslmed.3004666

von Economo, C.F., Koskinas, G.N., 1925. Die cytoarchitektonik der hirnrinde des erwachsenen menschen. J. Springer.

Wang, X., Studholme, C., Grigsby, P.L., Frias, A.E., Cuzon Carlson, V.C., Kroenke, C.D., 2017. Folding, But Not Surface Area Expansion, Is Associated with Cellular Morphological Maturation in the Fetal Cerebral Cortex. J. Neurosci. 37, 1971–1983. https://doi.org/10.1523/JNEUROSCI.3157-16.2017

Xu, G., Knutsen, A.K., Dikranian, K., Kroenke, C.D., Bayly, P.V., Taber, L.A., 2010. Axons Pull on the Brain, But Tension Does Not Drive Cortical Folding. Journal of Biomechanical Engineering 132, 071013. https://doi.org/10.1115/1.4001683

Yu, Q., Ouyang, A., Chalak, L., Jeon, T., Chia, J., Mishra, V., Sivarajan, M., Jackson, G., Rollins, N., Liu, S., Huang, H., 2016. Structural Development of Human Fetal and Preterm Brain CP Based on Population-Averaged Templates. Cereb. Cortex 26, 4381–4391. https://doi.org/10.1093/cercor/bhv201

Yun, H.J., Vasung, L., Tarui, T., Rollins, C.K., Ortinau, C.M., Grant, P.E., Im, K., 2020. Temporal Patterns of Emergence and Spatial Distribution of Sulcal Pits During Fetal Life. Cerebral Cortex 30, 4257–4268. https://doi.org/10.1093/cercor/bhaa053